Electronic Supplementary Material (ESI) for Inorganic Chemistry Frontiers.

Bifunctional atomically dispersed ruthenium electrocatalysts with ultralow metal loading for efficient bipolar membrane water electrolysis

Zhipeng Yu,[‡a,b,c] Chaowei Si,[‡d] Francisco Javier Escobar-Bedia,[e] Alec P. LaGrow,[a] Junyuan Xu,[f] Maria J. Sabater,[e] Isilda Amorim,[a] Ana Araujo,[a,b,c] Juliana P.S. Sousa,[a] Lijian Meng,[g] Joaquim Luis Faria,[b,c] Patricia Concepcion,[e] Bo Li [d,*] and Lifeng Liu [a,*]

[a]Clean Energy Cluster, International Iberian Nanotechnology Laboratory (INL), Avenida Mestre Jose Veiga, 4715-330 Braga, Portugal

[b]LSRE-LCM - Laboratory of Separation and Reaction Engineering - Laboratory of Catalysis and Materials, Faculty of Engineering, University of Porto, Rua Dr. Roberto Frias s/n 4200-465 Porto, Portugal

[c]ALiCE - Associate Laboratory in Chemical Engineering, Faculty of Engineering, University of Porto, Rua Dr. Roberto Frias s/n 4200-465 Porto, Portugal

[d]Shenyang National Laboratory for Materials Science, Institute of Metal Research, Chinese Academy of Sciences, Shenyang 110016, China

[e]Instituto de Tecnología Química, Universitat Politècnica de València-Consejo Superior de Investigaciones Científicas (UPV-CSIC), Avenida de los Naranjos s/n, 46022 Valencia, Spain

[f]Laboratory of Advanced Spectro-electrochemistry and Li-on Batteries, Dalian Institute of Chemical Physics, Chinese Academy of Sciences, 116023 Dalian, China.

[g]Centre of Innovation in Engineering and Industrial Technology, Instituto Superior de Engenharia do Porto, Instituto Politécnico do Porto, 4249-015 Porto, Portugal

[‡] Zhipeng Yu and Chaowei Si contributed equally to this work.

[*] Corresponding author: boli@imr.ac.cn (B. Li); lifeng.liu@inl.int (L. Liu)

Experimental procedures

Reagents

All reagents were used as received without further purification. Alginate acid, ammonia solution (NH_4OH), and Nafion® perfluorinated resin solution (5 wt %) were purchased from Sigma-Aldrich. Activated carbon (Norit CN-1) was bought from Fisher Scientific. Ruthenium chloride hydrate ($RuCl_3 \cdot xH_2O$) was acquired from Johnson Matthey. Potassium hydroxide (KOH) and ruthenium dioxide (RuO_2) powders were purchased from Alfa Aesar.

Synthesis of atomically dispersed Ru ADCs

The Ru ADCs were prepared through a two-step process involving the introduction of nitrogen groups by dispersing ammonium alginate onto a carbonaceous support, followed by the incorporation of the ruthenium precursor in an alcoholic solution and subsequent pyrolysis treatment.[S1-S3] Typically, 0.2 g of alginate acid was dissolved in 20 mL of deionized Milli-Q water (resistivity: 18.2 MΩ·cm), and 2 mL of NH_4OH (28 %) was then added in order to transform the insoluble acid to the soluble ammonium salt (NH_4A). Subsequently, 0.8 g of the activated carbon support (Norit CN-1) was added and the mixture was vigorously stirred for 1 h. The solvent was evaporated under vacuum at 65 °C and the dried product was ground into powders. The ground support (20 % NH_4A/C) composed of 20 wt% ammonium alginate was then dispersed in 10 mL of 1-butanol containing 5.3 mg of $RuCl_3 \cdot xH_2O$ (40 %) and kept at the reflux temperature of the alcohol (117.7 °C) for 16 h. Afterward, the Ru-impregnated solid was filtered, washed three times with 50 mL of ethanol and dried under reduced pressure at room temperature for 12 h. Finally, the as-prepared sample (0.2 wt% Ru-20 % NH_4A/C) was subjected to a pyrolysis treatment at 800 °C for 2 h under a N_2 flow of 50 mL min^{-1} with a ramping rate of 25 ºC min^{-1} to yield the Ru ADCs with 0.2 wt% Ru loading (i.e. Ru (0.2)-NC). Likewise, the pristine nitrogen-doped carbon (denoted

as NC hereafter) was prepared as a control sample, according to a similar procedure as described above, in the absence of ruthenium precursors.

Materials characterization

X-ray diffractometry (XRD) examinations were performed on an X'Pert PRO diffractometer (PANalytical) set at 45 kV and 40 mA with Cu K_α radiation (λ = 1.541874 Å) and a PIXcel detector. Data were collected in the Bragg-Brentano configuration in the 2θ range of 30 – 100° at a scan speed of 0.011° s^{-1}. X-ray photoelectron spectroscopy (XPS) characterization was carried out on an ESCALAB 250 instrument (Thermo Scientific) with Al K_α X-rays (1486.6 eV). Scanning electron microscopy (SEM) examination was conducted on a FEI Quanta 650 FEG microscope. Transmission electron microscopy (TEM), high-resolution TEM (HRTEM), and scanning transmission electron microscopy (STEM) elemental mapping investigations were carried out on a probe-corrected transmission electron microscope operating at 200 kV (FEI Themis 60-300). The Ru loading of Ru ADCs was determined by inductively coupled plasma-optical emission spectroscopy (ICP-OES, ICPE-9000 spectrometer, Shimadzu). Nitrogen adsorption/desorption porosimetry measurements were conducted using a Quantachrome Autosorb IQ_2 system at 77 K. The surface area of samples was derived by the Brunauer-Emmett-Teller (BET) method, and the pore size distribution was plotted by the Barrett-Joyner-Halenda (BJH) method.

DFT calculations

DFT calculations were performed using Vienna Ab-initio Simulation Package (VASP) with the projector augmented wave (PAW) pseudopotential and Revised Perdew-Burke-Ernzerhof (RPBE) functional.[S4-S6] A kinetic energy cut-off of 400 eV was adopted for the plane-wave expansion. A Gamma point was used to sample the Brillouin zone in energy and structure relaxation calculation. A 3 × 3 × 1 Monkhorst-Pack k-point mesh was utilized in electronic structure calculations. All

structures were fully relaxed until the final energy and force on each atom were less than 10^{-6} eV and 0.02 eV $Å^{-1}$, respectively. A 5 × 6 supercell including 62 C, 4 N and 1 Ru atoms, was chosen for modelling atomically dispersed Ru, while in the N-doped graphene sheet model, the graphene supercell is 14.76 × 12.75 × 15.00 $Å^3$ in the x, y and z directions and the periodic condition is applied along z direction. The following catalyst models were used for the calculations: Ru single atom with the pyrrolic N coordination configuration; Ru single atom with the pyridinic N coordination configuration; Pt (111) surface for the HER; RuO_2 (110) surface for the OER. The HER proceeds through the two-electron pathways with the following reaction steps:

$$^* + H^+ + e^- \rightarrow H^* \quad (1)$$

$$H^* + H^+ + e^- \rightarrow H_2\,(g) + ^* \quad (2a)$$

$$\text{or} \quad H^* + H^* \rightarrow H_2\,(g) + 2^* \quad (2b)$$

The OER process includes the following steps:

$$^* + OH^- \rightarrow OH^* + e^- \quad (3)$$

$$OH^* + OH^- \rightarrow O^* + H_2O\,(l) + e^- \quad (4)$$

$$O^* + OH^- \rightarrow OOH^* + e^- \quad (5)$$

$$OOH^* + OH^- \rightarrow ^* + O_2\,(g) + H_2O\,(l) + e^- \quad (6)$$

where * represents the Ru active site, and OH^*, O^*, OOH^* and H^* are the intermediates absorbed on the active sites during the OER and HER. The adsorption energy was calculated as follows: $E_{ad} = E_{sys} - E_{sur} - E_{spe}$, in which E_{ad}, E_{sys}, E_{sur} and E_{spe} denote the adsorption energy, the energy of adsorption system, the energy of clean surface, and the energy of insulated adsorption species, respectively.

Electrode preparation and electrocatalytic tests

To prepare the working electrode, 5 mg of Ru (0.2)-NC catalysts was first ultrasonically dispersed into 500 µL of ethanol and 50 µL of Nafion® (Sigma, 5 wt%) solution to form a homogeneous ink. Subsequently, 6.6 µL of catalyst ink was loaded on a polished glassy carbon (GC) electrode with an exposed area of 0.2 cm^2, resulting in a Ru loading density of 0.6 µg cm^{-2}. For comparison, the electrocatalytic performance of commercial Pt/C (FuelCellStore, 20 wt% Pt), RuO_2 nanoparticles (Alfa Aesar) and pristine NC support control samples was also investigated. The working electrode was prepared according to the procedure similar to that described above. The metal loading density of Pt/C and RuO_2 was 60 and 300 µg cm^{-2}, respectively.

All electrocatalytic tests were performed in a three-electrode configuration at room temperature using a Biologic VMP-3 potentiostat/galvanostat. A graphite rod and a saturated calomel electrode (SCE) were utilized as the counter and reference electrodes, respectively. Unless otherwise stated, all potentials are reported versus the reversible hydrogen electrode (RHE) by converting the measured potentials according to the following equation:

$$E_{RHE} = E_{SCE} + 0.059 \times pH + 0.241 \quad (7)$$

The apparent HER and OER activities were appraised using linear scan voltammetry (LSV) at a scan rate of 5 mV s^{-1}, and an *iR*-correction (85%) was applied to compensate for the voltage drop between the reference and working electrodes, which was measured by a single-point high-frequency impedance measurement.

The electrocatalytically-active surface areas (ECSAs) were estimated from the electrochemical double-layer capacitance (C_{dl}) of the catalysts. The C_{dl} values were derived by performing cyclic voltammetry (CV) in the non-Faradaic potential range of 0.4 – 0.6 V *vs.* RHE at different scan rates (v) of 10, 20, 30, 40, 50, 60, 70, 80, 90 and 100 mV s^{-1}, followed by extracting the slope from

the resulting $|j_a - j_c|/2$ *vs.* v plots (j_a and j_c represent the anodic and cathodic current at 0.5 V *vs.* RHE). The ECSA was computed according to the following formula:[S7]

$$ECSA = \frac{C_{dl}}{C_s} \quad (8)$$

where C_s represents the areal capacitance of a flat surface (35 μF cm^{-2}).[S8]

Electrochemical impedance spectroscopy (EIS) measurements were carried out at –0.047 V *vs.* RHE for HER in 0.5 M H_2SO_4, –0.073 V *vs.* RHE for HER in 1.0 M KOH and 1.530 V *vs.* RHE for OER in 1.0 M KOH in the frequency range of 10^5 – 0.01 Hz with a 10 mV sinusoidal perturbation. The stability of catalysts was assessed at a constant current density of –10 mA cm^{-2} for HER and 10 mA cm^{-2} for OER using chronopotentiometry (CP).

For HER and OER, the turnover frequency (TOF) of the catalysts was calculated according to the following formula:[S9]

HER: $$TOF = \frac{j}{2nF} \quad (9)$$

OER: $$TOF = \frac{j}{4nF} \quad (10)$$

where j (A) is the current at a given overpotential, F = 96500 C mol^{-1} stands for the Faraday constant, and n (mol) is mole number of Ru or Pt loaded on the GC electrode. All metal species in catalysts were assumed to be catalytically active, so the calculated values represent the lower limits of TOF.

Overall water splitting performance

The overall water electrolysis performance was firstly investigated in a two-compartment Teflon cell using Ru ADCs as both HER and OER catalysts in the presence of an anion exchange membrane (AEM). 1.0 M KOH solution was used as the electrolyte. Furthermore, asymmetric water electrolysis in acid-alkaline dual electrolytes was also demonstrated using a bipolar

membrane (BPM) to separate the cathodic compartment from the anodic one. In this case, 1.0 M KOH and 0.5 M H_2SO_4 were supplied as the anolyte and catholyte, respectively. For comparison, commercial Pt/C and RuO_2 were also utilized as HER and OER catalysts, respectively, and tested in the same asymmetric configuration. The Faradaic efficiency of the hydrogen and oxygen evolution was measured during the continuous BPM water electrolysis at 10 mA cm^{-2}. The stability of overall water electrolysis was assessed in the two-compartment Teflon cell using CP at a constant current density of 10 mA cm^{-2}.

Supplementary figures:

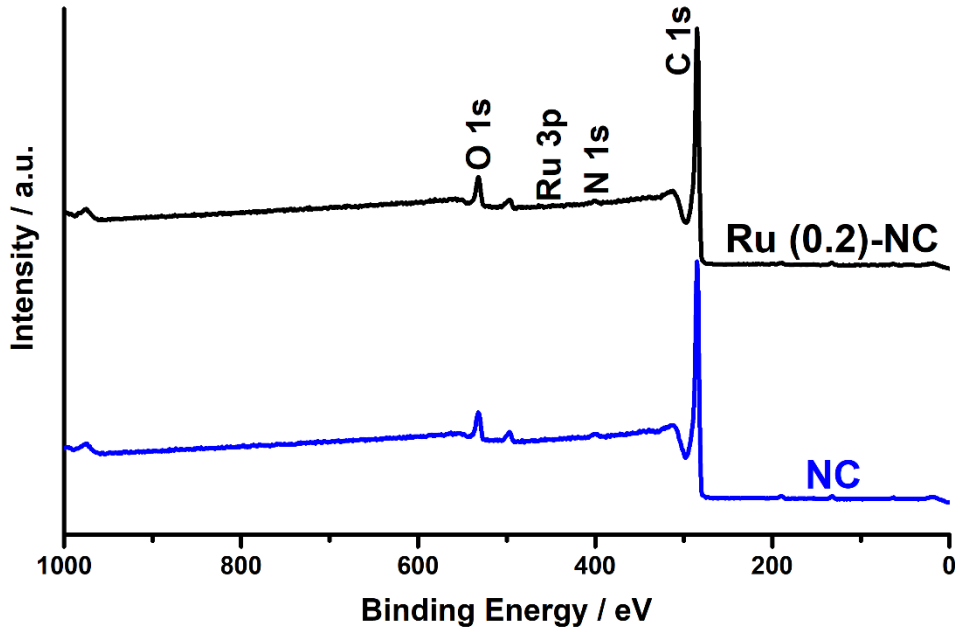

Fig. S1. XPS survey spectra of Ru (0.2)-NC and pristine NC.

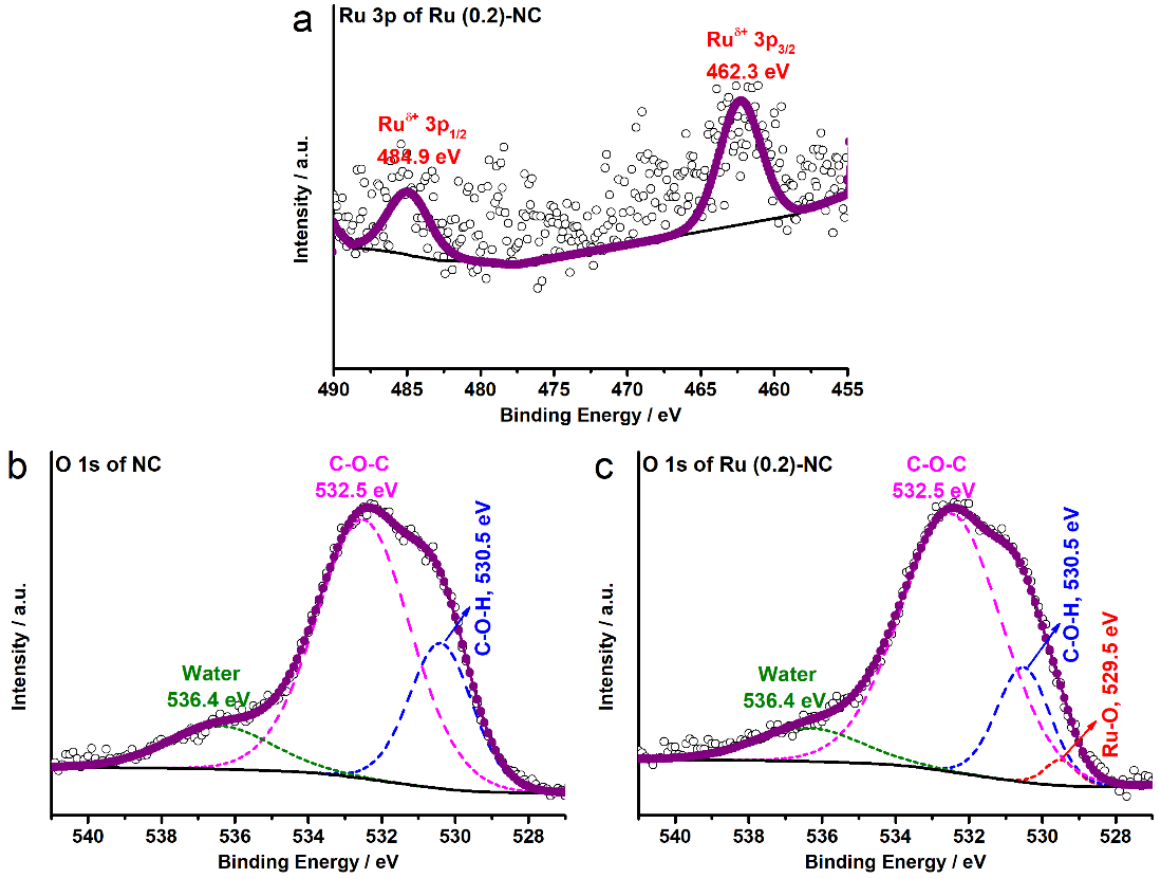

Fig. S2. a) Ru3p XPS spectrum of Ru (0.2)-NC. O1s XPS spectra of b) pristine NC and c) Ru (0.2)-NC.

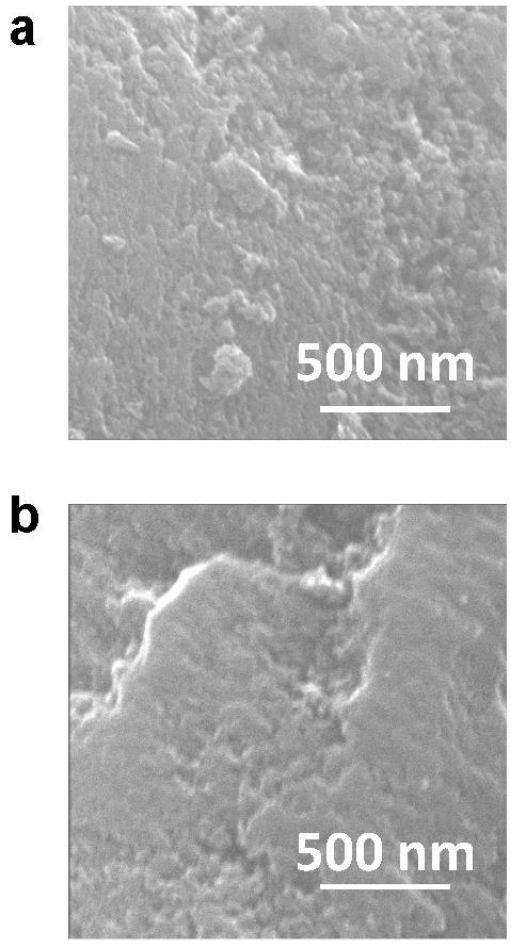

Fig. S3. SEM images of a) pristine NC and b) Ru (0.2)-NC.

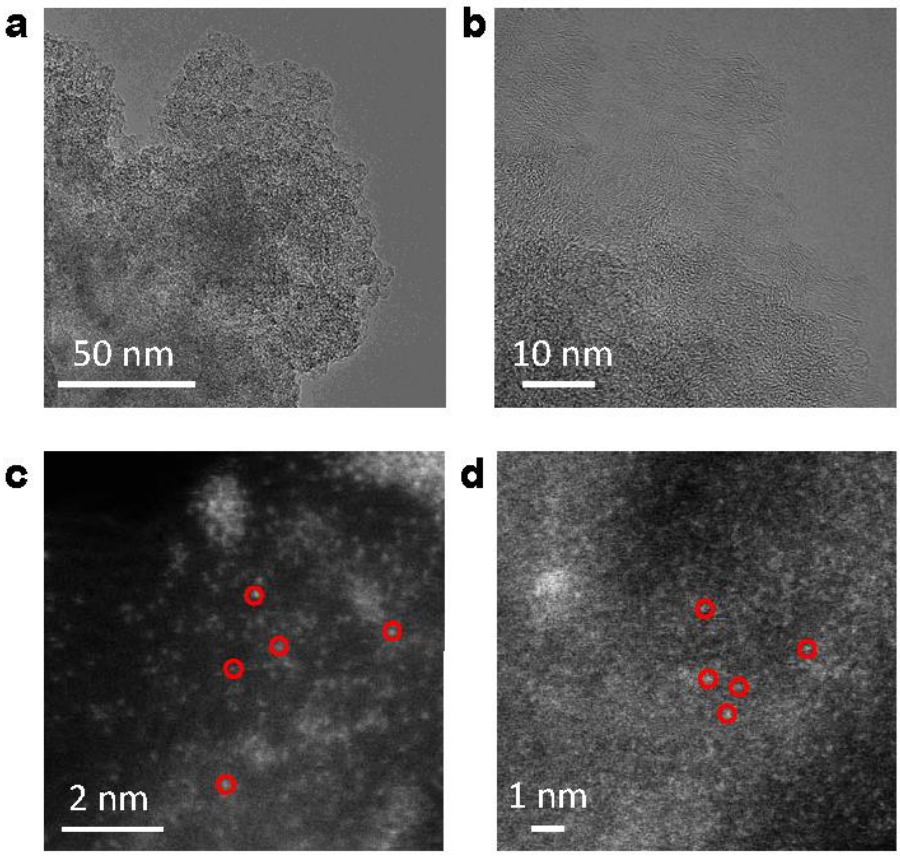

Fig. S4. a) Low- and b) high-magnification HRTEM images of Ru (0.2)-NC. (c, d) HAADF-STEM images of Ru (0.2)-NC, where some nanometric clusters can be distinguished.

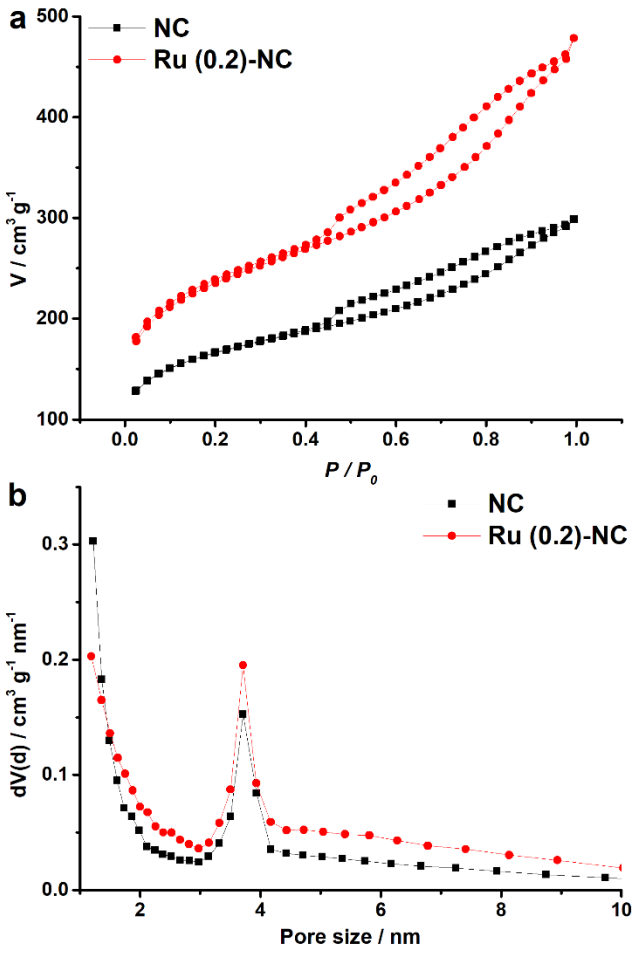

Fig. S5. (a) N_2 adsorption and desorption isotherms and (b) pore size distribution of Ru (0.2)-NC and pristine NC.

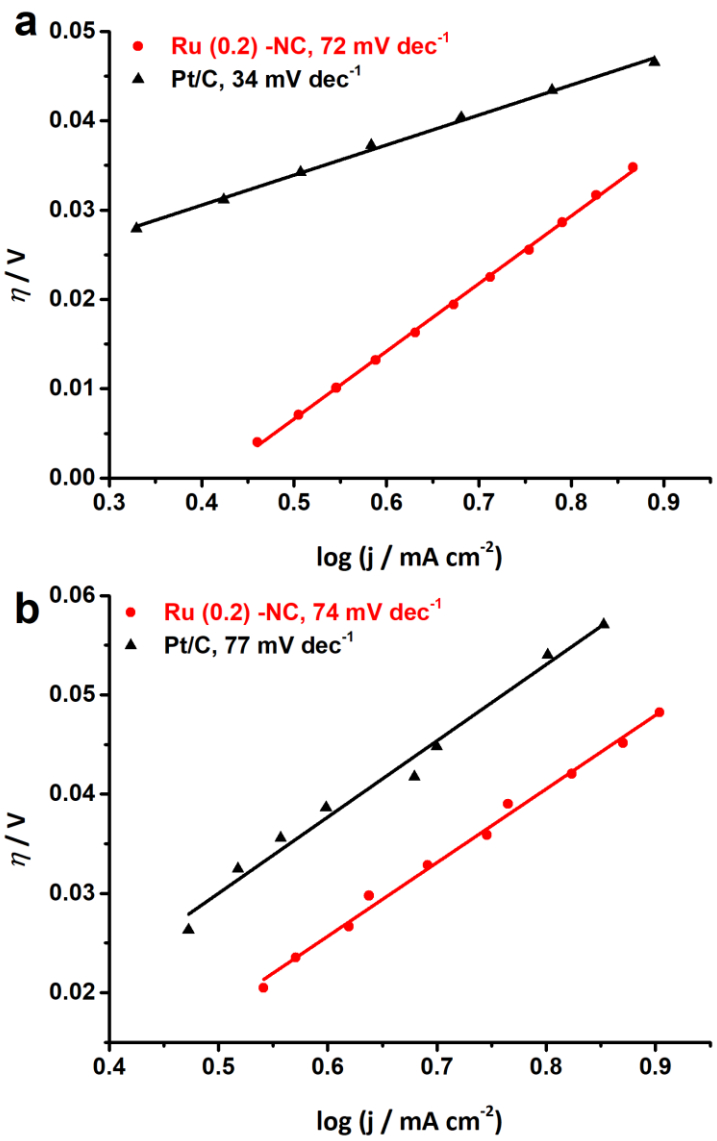

Fig. S6. Tafel slopes of the catalysts derived from electrocatalytic tests in a) 0.5 M H_2SO_4 and b) 1.0 M KOH.

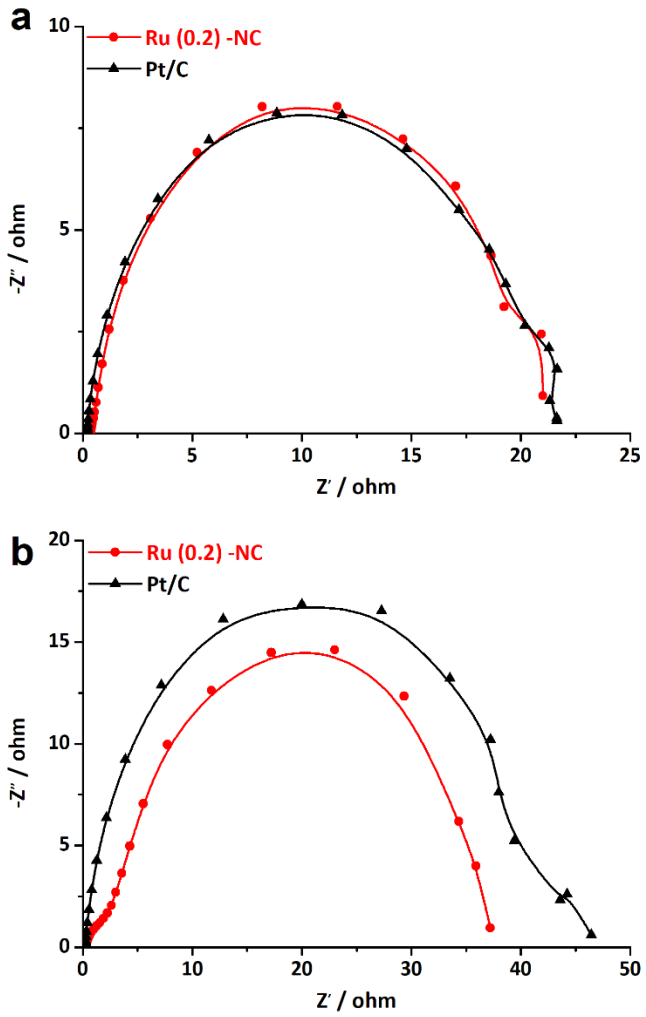

Fig. S7. Nyquist plots of the catalysts toward HER tested in a) 0.5 M H_2SO_4 and b) 1.0 M KOH.

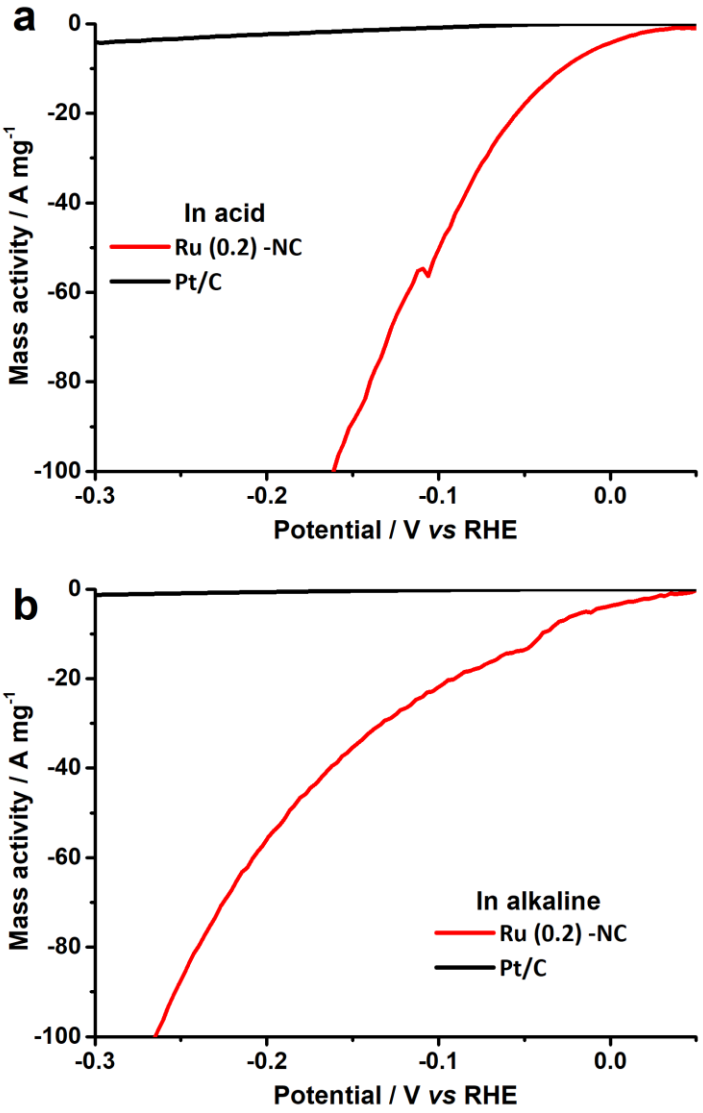

Fig. S8. Mass activities of Ru (0.2)-NC and commercial Pt/C catalysts toward HER tested in a) 0.5 M H_2SO_4 and b) 1.0 M KOH.

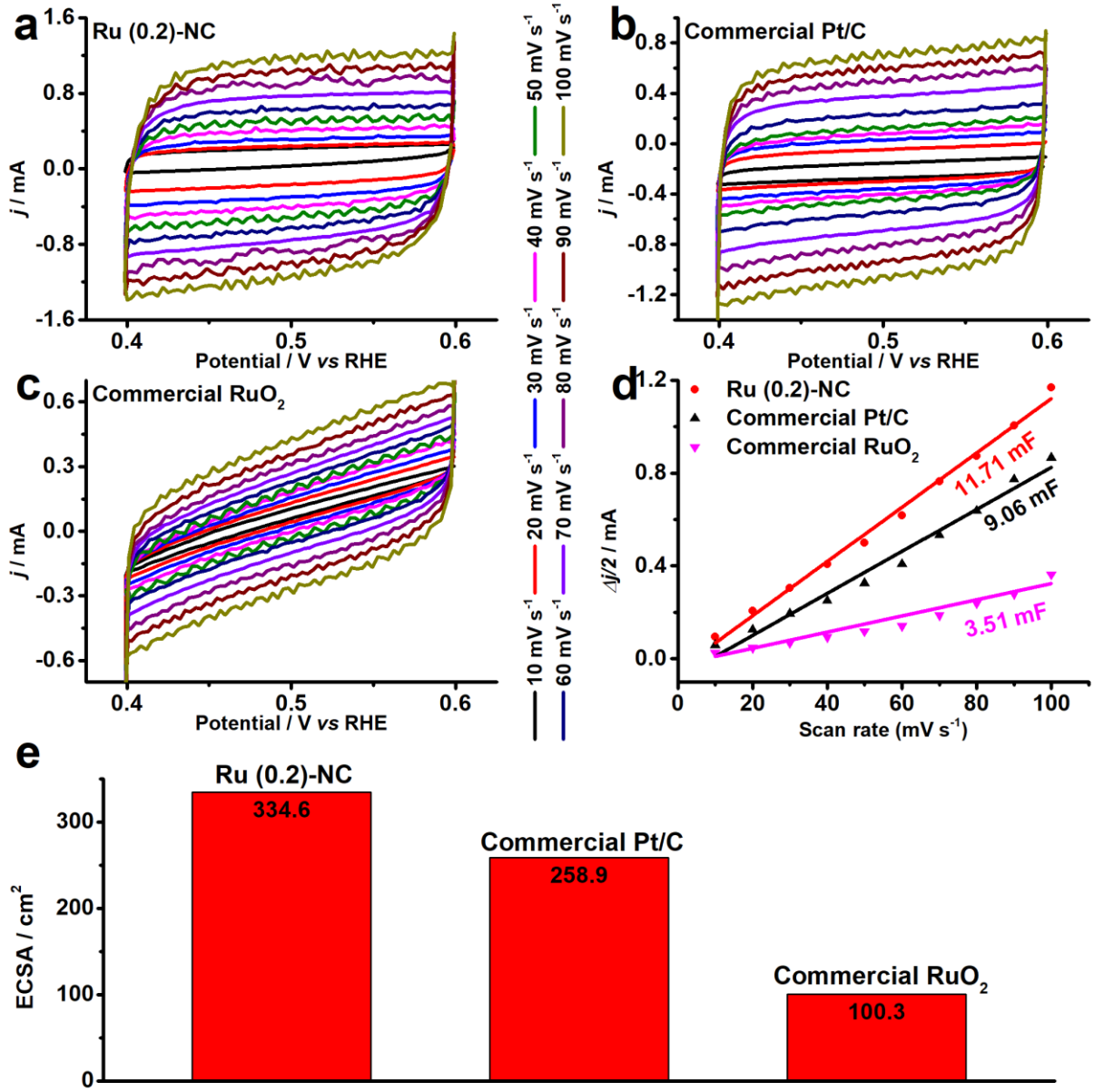

Fig. S9. Electrochemical CV curves of a) Ru (0.2)-NC, b) commercial Pt/C and c) commercial RuO_2, recorded at different scan rates of 10, 20, 30, 40, 50, 60, 70, 80, 90 and 100 mV s^{-1}. d) Plots of the capacitive currents as a function of the scan rate for all catalysts. e) ECSA of all catalysts.

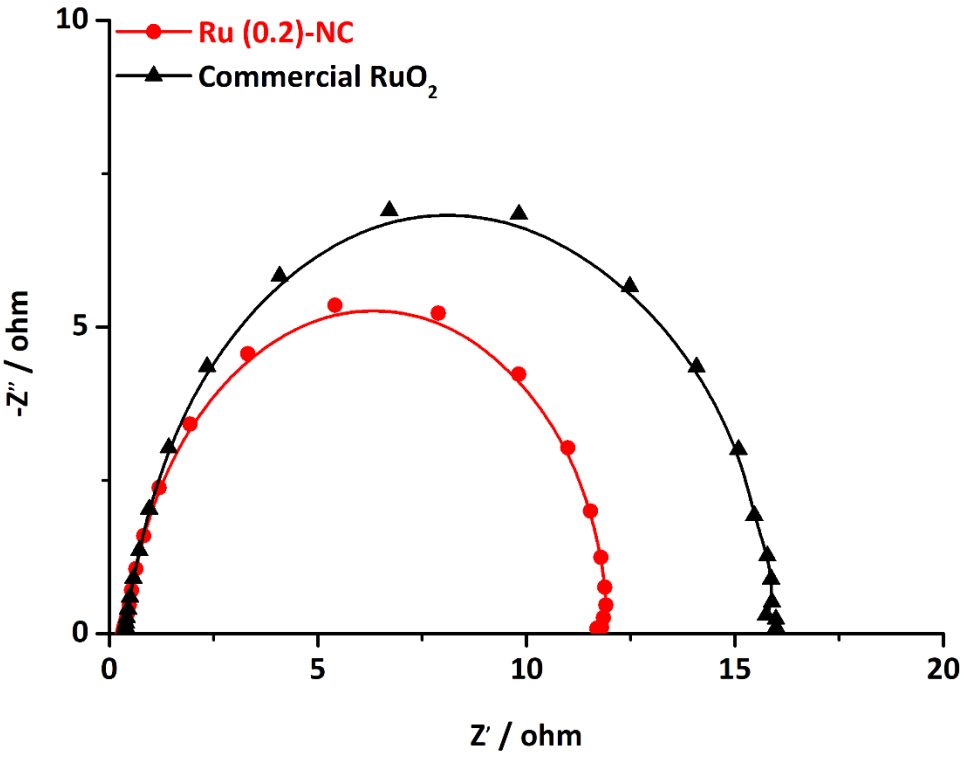

Fig. S10. Nyquist plots of the catalysts toward OER, measured at 1.53 V *vs* RHE in 1.0 M KOH.

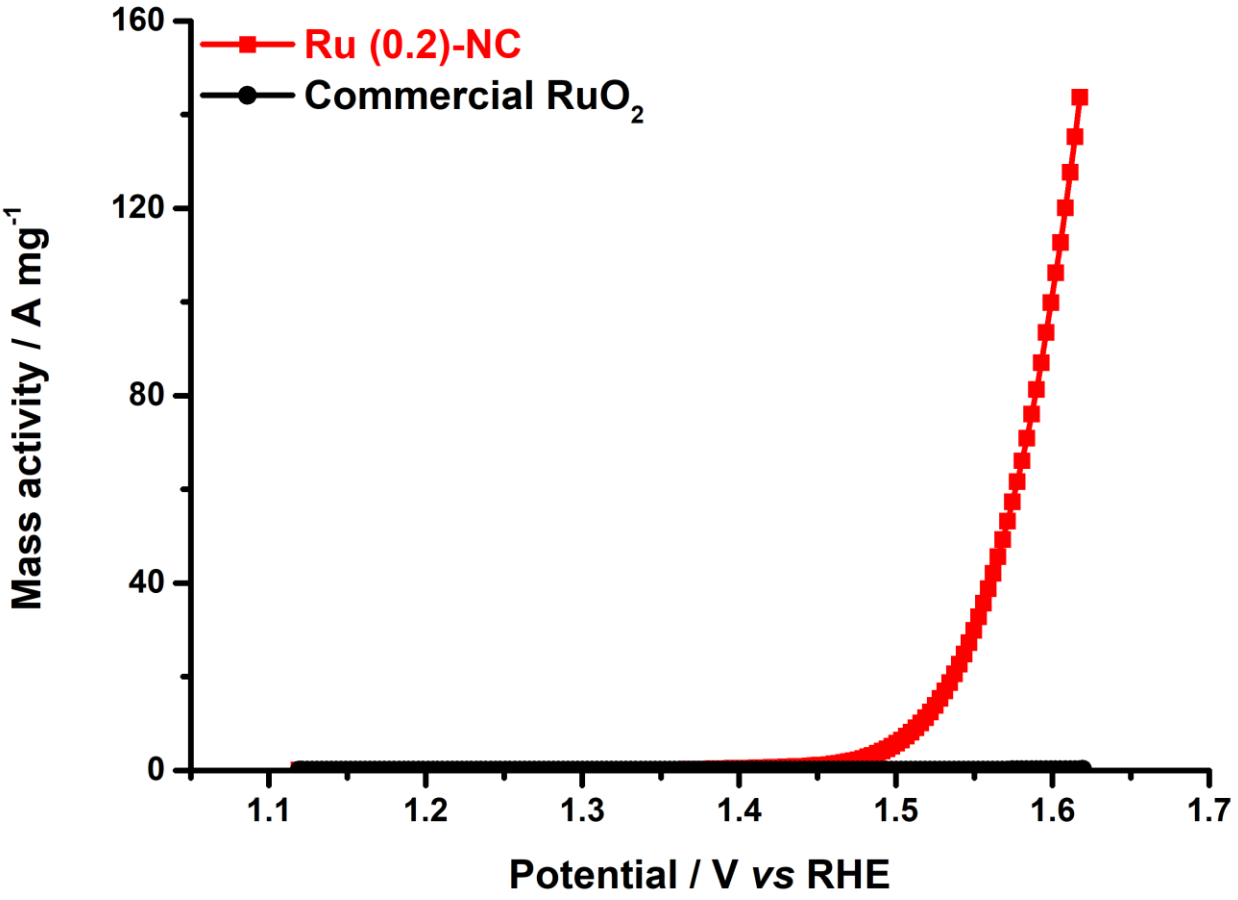

Fig. S11. Mass activities of Ru (0.2)-NC and commercial RuO_2 catalysts toward OER tested in 1.0 M KOH.

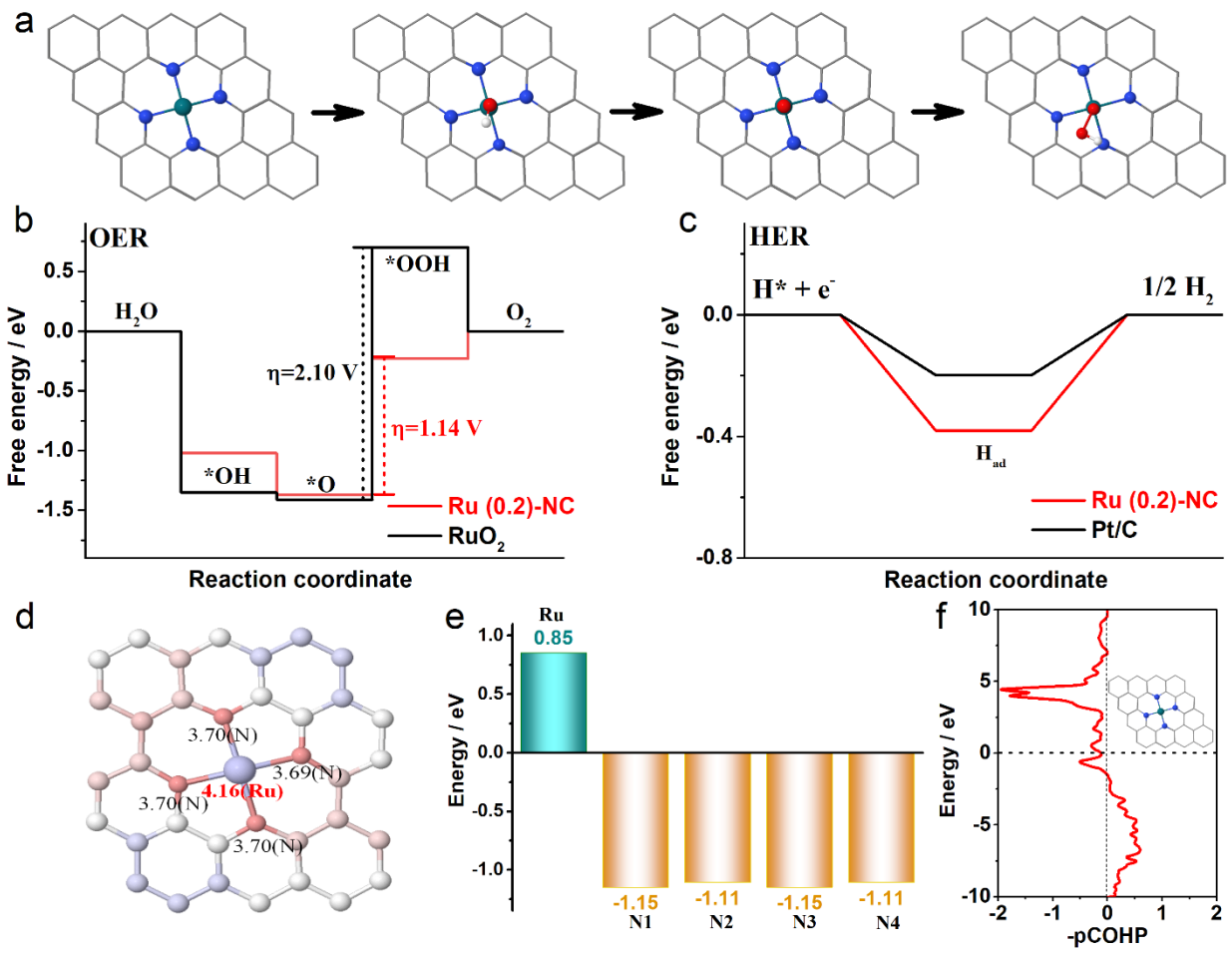

Fig. S12. (a) Adsorption configurations of the intermediates during the OER process on pyridinic-type Ru (0.2)-NC (the balls in cyan, blue, red and white represent Ru, N, O and H atoms, respectively). (b) Gibbs free-energy diagram for the four steps of OER and (c) two steps of HER on pyridinic-type Ru (0.2)-NC. (d) The band-order, (e) Bader charge and (f) COHP analysis in pyridinic-type Ru (0.2)-NC.

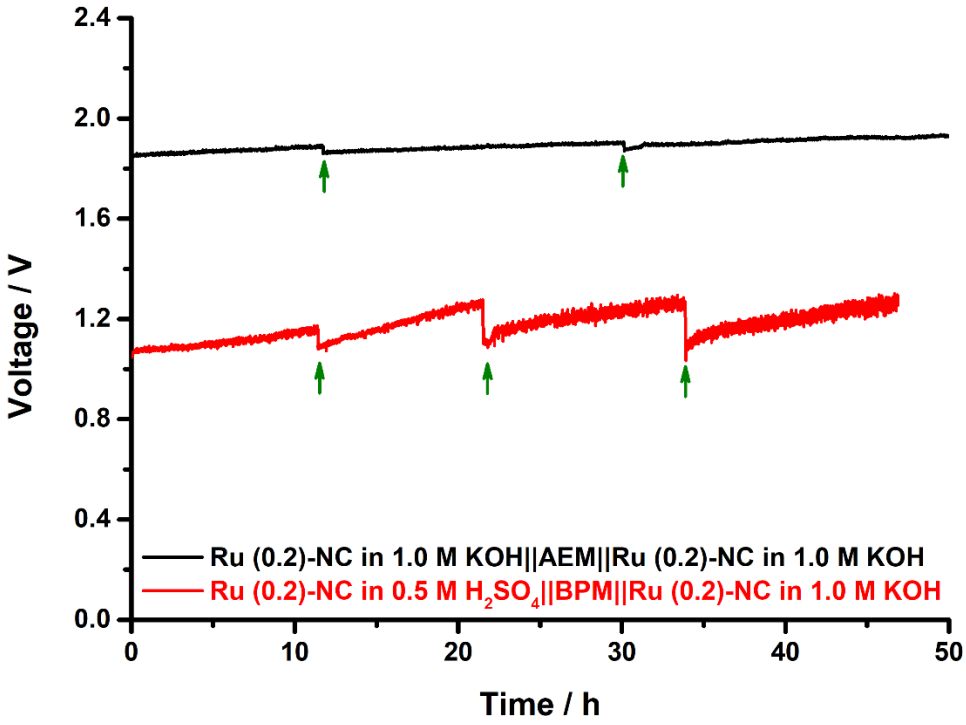

Fig. S13. Operational stability of AEMWE and BPMWE for Ru (0.2)-NC at 50 mA cm^{-2}. The arrows indicate the fluctuations arising from the replenishment of electrolyte.

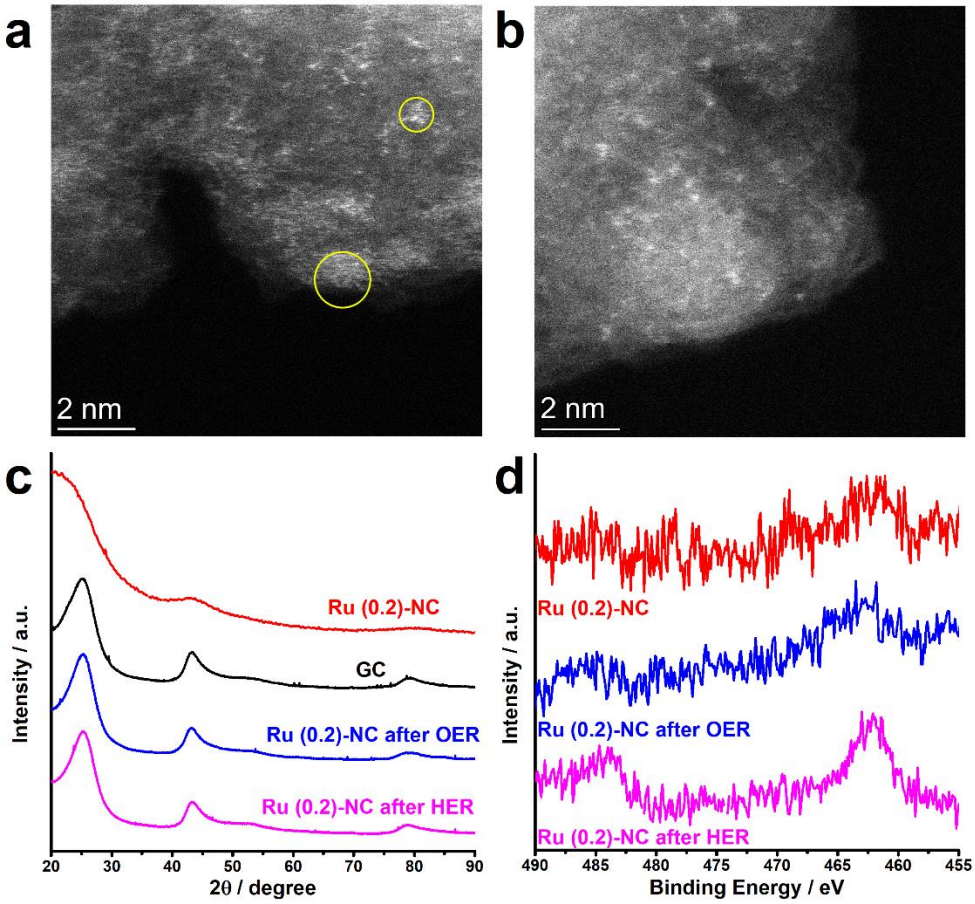

Fig. S14. STEM images of Ru (0.2)-NC upon a) the OER (anode) and b) the HER (cathode) during the extended BPMWE test at 10 mA cm^{-2}. Some clusters are observed after the test, as marked in yellow circles. c) XRD patterns and d) high-resolution Ru 3p spectra of Ru (0.2)-NC after the stability test. The XRD patterns of Ru (0.2)-NC after the stability test were collected with glassy carbon (GC) as the support, and therefore the diffraction peaks from GC are clearly visible in these patterns.

Supplementary tables:

Table S1. The surface composition of pristine NC and Ru (0.2)-NC.

Samples	C	N	O	Ru
NC	93.7	1.1	5.2	/
Ru (0.2)-NC	93.0	1.3	5.5	0.2

Table S2. Fitting results of the N1s spectrum in pristine NC and Ru (0.2)-NC.

Samples	Pyridinic N	M-N	Pyrrolic N	Graphitic N	Oxidized N
NC	26.3	/	38.8	29.1	5.8
Ru (0.2)-NC	20.9	10.7	5.3	44.4	18.7

Table S3. Comparison of the turnover frequencies (TOFs) of Ru (0.2)-NC to those of other recently reported Ru-based HER catalysts tested in acidic condition.

Catalyst	Overpotential (V)	TOF (s^{-1})	Reference
Ru (0.2)-NC	**0.1**	**26.2**	***This work***
Ru-HPC	0.025	0.18	*Nano Energy*, 2019, **58**, 1–10
Ru@C_2N	0.025	0.67	*Nat. Nanotechnol.*, 2017, **12**, 441-446
Ru@MWCNT	0.025	0.70	*Nat. Commun.*, 2020, **11**, 1278.
$RuCeO_2$	0.027	0.8	*ACS Appl. Mater. Interfaces*, 2018, **10**, 6299–6308
Ru-CCS	0.05	3.7	*J. Mater. Chem. A*, 2018, **6**, 2311–2317
Ru@GnP	0.1	0.26	*Adv. Mater.*, 2018, **30**, 1803676
Ru-Ni@Ni_2P-HNRs	0.1	1.1	*J. Am. Chem. Soc.*, 2018, **140**, 2731–2734
Ru/g-C_3N_4/C	0.1	4.85	*J. Am. Chem. Soc.*, 2016, **138**, 16174–16181
Ru-ENG	0.02	0.75	*Nano Energy, 2020, **76**, 105114*
Ru@Co/N-CNTs-2	0.1	0.56	*ACS Sustainable Chem. Eng., 2020, **8**, 9136–9144*
RuCoP	0.1	10.95	*Energy Environ. Sci., 2018, **11**, 1819*
Pt/C	0.015	0.30	*ACS Energy Lett., 2021, **6**, 1175–1180*

Table S4. Comparison of the turnover frequencies (TOFs) of Ru (0.2)-NC to those of other recently reported Ru-based HER catalysts tested in alkaline condition.

Catalyst	Overpotential (V)	TOF (s^{-1})	Reference
Ru (0.2)-NC	**0.1**	**11.5**	***This work***
Ru@MWCNT	0.025	0.40	*Nat. Commun.*, 2020, **11**, 1278.
Ru@C_2N	0.025	0.76	*Nat. Nanotechnol.*, 2017, **12**, 441-446
Ru/C	0.04	0.18	*Adv. Energy Mater.*, 2018, **8**, 1801698
Ru@GnP	0.1	0.145	*Adv. Mater.*, 2018, **30**, 1803676
Ru/NG-750	0.1	0.35	*ACS Appl. Mater. Interfaces*, 2017, **9**, 3785–3791
Ru-ENG	0.02	0.84	*Nano Energy, 2020, **76**, 105114*
Ru@Co/N-CNTs-2	0.05	0.25	*ACS Sustainable Chem. Eng. 2020, **8**, 9136–9144*
np-$Cu_{53}Ru_{47}$	0.1	1.139	*ACS Energy Lett. 2020, **5**, 192−199*
RuNi NSs	0.05	1.60	*Nano Energy, 2019, **66**, 104173*
Ru-ZIF-900	0.1	9.38	*J. Mater. Chem. A, 2020, **8**,3203-3210*
Ru/g-C_3N_4/C	0.1	4.2	*J. Am. Chem. Soc., 2016, **138**, 16174-16181*
Ru@NC-0.2	0.05	3.02	*Angew. Chem. Int. Ed., 2018, **57**, 5848-5852.*
Ru/NC	0.1	4.55	*J. Mater. Chem. A, 2017, **5**, 25314-25318.*
RuCoP	0.1	7.26	*Energy Environ. Sci., 2018, **11**, 1819*

Table S5. Comparison of turnover frequencies (TOFs) of Ru (0.2)-NC to those of other recently reported Ru-based OER catalysts tested in alkaline condition.

Catalyst	Overpotential (V)	TOF (s^{-1})	Reference
Ru (0.2)-NC	**0.30**	**4.89**	***This work***
$(Ru\text{-}Co)O_x$	0.27	0.252	*Angew. Chem. Int. Ed. 2020, **59**, 17219–17224*
Ru^0/CeO_2	0.35	0.004	*J. Colloid Interface Sci.,2019, **534**, 704-710*
Ru-NiFe-MOF/NF	0.28	0.506	*Dalton Trans., 2021,**50**, 4280-4287*
Ru-NiFeP/NF	0.25	0.190	*Appl. Surf. Sci., 2021, **536**, 147952*
RuCo@NC-750	0.30	0.35	*Electrochimica Acta, 2019, **327**, 134958*
NiRu@MWCNTs	0.30	1.12	*ACS Appl. Mater. Interfaces 2020, **12**, 13842–13851*

References

S1. A. Corma, P. Concepción, I. Domínguez, V. Forné and M. J. Sabater, *J. Catal.*, 2007, **251**, 39-47.

S2. M. J. Sabater, T. Ródenas and A. Heredia, in *Handbook of Biopolymer-Based Materials*, pp. 37-86.

S3. F. J. Escobar-Bedia, M. Lopez-Haro, J. J. Calvino, V. Martin-Diaconescu, L. Simonelli, V. Perez-Dieste, M. J. Sabater, P. Concepción and A. Corma, *ACS Catal.*, 2022, 4182-4193.

S4. G. Kresse and J. Furthmüller, *Phys. Rev. B*, 1996, **54**, 11169-11186.

S5. P. E. Blöchl, *Phys. Rev. B*, 1994, **50**, 17953-17979.

S6. J. P. Perdew, K. Burke and M. Ernzerhof, *Phys. Rev. Lett.*, 1996, **77**, 3865-3868.

S7. J. Xu, J. Li, Z. Lian, A. Araujo, Y. Li, B. Wei, Z. Yu, O. Bondarchuk, I. Amorim, V. Tileli, B. Li and L. Liu, *ACS Catal.*, 2021, **11**, 3402-3413.

S8. C. C. L. McCrory, S. Jung, J. C. Peters and T. F. Jaramillo, *J. Am. Chem. Soc.*, 2013, **135**, 16977-16987.

S9. I. Amorim, J. Xu, N. Zhang, Z. Yu, A. Araújo, F. Bento and L. Liu, *Chem. Eng. J.*, 2021, **420**, 130454.